The petrosal and basicranial morphology of *Protoceras celer*

Short title: *Protoceras celer* petrosal morphology

Selina Viktor Robson[1]*, Brendon Seale[2], Jessica M. Theodor[1]

[1] Department of Biological Sciences, University of Calgary, Calgary, Alberta, Canada

[2] Lunenfeld-Tanenbaum Research Institute, Sinai Health System, Toronto, Ontario, Canada

Abstract

Protoceratids are an extinct family of endemic North American artiodactyls. The phylogenetic position of protoceratids in relation to camelids and ruminants has been contentious for over a century. The petrosal morphology of basal (*Leptotragulus*) and derived (*Syndyoceras*) protoceratids has suggested that protoceratids are closely related to ruminants, whereas a prior description of a disarticulated intermediate protoceratid petrosal (*Protoceras celer*) indicated that protoceratids were closely related to camelids. This contradictory evidence implied that there were several character reversals within the protoceratid lineage and brought into question the utility of basicranial characters in artiodactyl phylogenetics. Here, we provide descriptions of an additional *P. celer* petrosal. The descriptions are based on data produced by computed tomography scans, which allowed us to image the petrosal *in situ* in the skull. Our results indicate that the petrosal morphology of *P. celer* is similar to that of other protoceratids, implying that, contrary to previous evidence, petrosal morphology is conserved within the Protoceratidae.

Introduction

The Protoceratidae represent an early lineage of North American artiodactyls with elaborate cranial ornamentation. Several of the most basal taxa are hornless, but males of more derived species bear horns on the frontals, parietals, nasals, and/or the occiput [1–3]. Females typically lack horns but bear rough patches in the same locations [2]. Protoceratids range in body mass from 20 kg to 350 kg and are also sexually dimorphic with respect to overall body size [3].

Protoceratids first appeared in the middle Eocene (early Uintan) and persisted into the early Pliocene (latest Hemphillian) of North and Central America [4]. The family is subdivided into the "Leptotragulinae", the Protoceratinae, and the Synthetoceratinae [5]. The "leptotragulines" are a paraphyletic assemblage of basal Eocene hornless forms [4]. The protoceratines consist of most of the smaller horned taxa, including *Protoceras.* Known protoceratine taxa range from the early Oligocene (Whitneyan) to the late Miocene (Clarendonian) [2]. Synthetoceratines first appeared in the early Miocene (early late Arikareean) and persisted until the early Pliocene (late Hemphillian) [6]. The synthetoceratines are larger-bodied, derived protoceratids characterized by their rostral "slingshot" and orbital horns in the males.

Apart from the presence of cranial appendages, protoceratids exhibit a morphology typical of generalized selenodont artiodactyls, including a basic selenodont dentition. Protoceratids have elongated limbs and a fused ectomesocuneiform, but their cuboid and navicular remain separate and their metapodial keels are incomplete [4]. Protoceratines and synthetoceratines have a complete postorbital bar, but this condition is not present in basal members of the family [7].

The phylogenetic affinities of protoceratids have been the subject of considerable dispute. Protoceratids were originally allied with ruminants, a view that persisted for half a century [8–16]. Like ruminants, protoceratids lack upper incisors and possess an incisiform lower canine. The protoceratid auditory bulla is hollow and is compressed between the glenoid fossa and the exoccipital. Yet protoceratids lack a cubonavicular, one of the most distinctive ruminant synapomorphies [17].

"Leptotragulines" have historically been placed in Tylopoda [11–13], but the more derived protoceratids were not allied with camelids (and other tylopods) until the mid-twentieth century [2,6,18–24]. This shift in systematics was largely driven by morphological similarities between protoceratids and camelids. It is now understood that most of these similarities are plesiomorphic (e.g., incomplete metapodial keels, unfused cuboid and navicular) or homoplastic (e.g., elongate limbs, complete postorbital bar). The one unusual morphology shared by protoceratids and camelids is the location of the vertebrarterial canal—both families have a vertebral artery canal that passes through the pedicles of the cervical vertebrae. This condition is only found in camelids, protoceratids, and the endemic European xiphodontids [4,21]. However, protoceratids lack other morphologies that have been associated with camelids, such as the presence of a dorsally-projecting angular hook on the dentary and an inflated auditory bulla filled with cancellous bone [4].

This conflicting osteological evidence has presented challenges for inferring protoceratid relationships. At the turn of the twenty-first century, novel information became available; the endocranial morphology of the basal "leptotraguline" protoceratid *Leptotragulus* and the derived synthetocerine protoceratid *Syndyoceras* were described. The morphology of *Syndyoceras* was described from computed tomography (CT) scans [25] and the morphology of *Leptotragulus* was described from physical dissections of the fossil [7]. Based on these descriptions, Joeckel, Stavas, and Norris all concluded that protoceratid endocranial morphology is more similar to that of ruminants than to that of camelids, suggesting that early workers may have been correct in placing protoceratids with ruminants [7,25].

An additional description of a protoceratid petrosal was provided in an American Museum of Natural History monograph [26]. This detailed description was of AMNH-VP 645, a skull and disarticulated petrosal attributed to *Protoceras celer* [26]. This specimen, in contrast to the UNSM 1153 *Syndyoceras* material and the YPM and MCZ *Leptotragulus* material described by Joeckel and Stavas [25] and Norris [7], showed a deep subarcuate fossa and no sharp demarcation ridge along the endocranial face of the petrosal. The petrosal characters for *P. celer* were coded in a phylogenetic analysis based on AMNH-VP 645 [27]. The total evidence phylogenetic analysis recovered protoceratids in a position within Ruminantia, but the morphological phylogenetic analysis recovered protoceratids in a position close to camelids, supporting the interpretation that protoceratids are tylopods [27].

The description of AMNH-VP 645 calls into question characters for *Syndyoceras* [25] and differs from the description of *Leptotragulus* [7]. There are two potential explanations for these discrepancies: *P. celer* represents several character state reversals within Protoceratidae, or the AMNH-VP 645 petrosal is incorrectly attributed to *P. celer*. We tested these explanations by subjecting two skulls of *P. celer* [AMNH-VP 1229; AMNH-VP 53523] to CT scanning and reconstructed the petrosal from the CT scan data. Our results indicate that AMNH-VP 53523 has a petrosal morphology like that of other protoceratids, implying that the AMNH-VP 645 petrosal was incorrectly referred to *P. celer*.

Materials and Methods

Institutional Abbreviations—AMNH-VP, American Museum of Natural History, New York; UCMZ, University of Calgary Museum of Zoology, University of Calgary; MCZ, Museum of Comparative Zoology, Harvard University; UNSM, University of Nebraska State Museum

paleontology collections, University of Nebraska, Lincoln; YPM, Yale Peabody Museum, Yale University; ZM, University of Nebraska State Museum mammalogy collections.

Material—AMNH-VP 1229 and AMNH-VP 53523 are skulls, referred to *Protoceras celer*, from the Poleside member of the Brule Formation, South Dakota, both of Whitneyan age [2]. The right side of AMNH-VP 1229 has minor dorsoventral compression, but the specimen is mostly complete. There is slight damage to the dorsal skull roof, and the ventral portion of the left orbit is missing. AMNH-VP 1229 is identified as a female because it lacks the cranial ornamentation present in males and is smaller in size (Fig 1A-C).

Fig 1. Photographs of the *Protoceras celer* specimens included in this study.

(A) Ventral view of AMNH 1229. (B) Dorsal view of AMNH 1229. (C) Right lateral view of AMNH 1229. (D) Ventral view of AMNH 53523. (E) Dorsal view of AMNH 53523. (F) Right lateral view of AMNH 53523.

AMNH-VP 53523 has not been completely prepared and matrix remains on much of the basicranium. The skull is crushed dorsoventrally but maintains its original width. Cranial appendages are present but damaged, aside from the intact right rostral horn. AMNH-VP 53523 is identified as a male because of the presence of cranial appendages and larger size (Fig 1D-F).

Computed Tomography Scan—AMNH-VP 1229 and AMNH-VP 53523 were subjected to micro-computed tomography (µCT) scanning at the High-Resolution Computed Tomography Facility at the University of Texas at Austin. Both skulls were initially scanned at a 0.5 mm thickness using the P250D x-ray detector operating at 419 kV and 1.8 µA. These scans produced a stack of 140 images for AMNH-VP 1229 and a stack of 151 images for AMNH-VP 53523, both at a resolution of 1024 x 1024. AMNH-VP 1229 was found to have several high-density deposits in the

basicranial region. These high-density deposits distorted the CT images and removed AMNH-VP 1229 as a candidate for high-resolution imaging.

The basicranium of AMNH-VP 53523 was subsequently scanned at a thickness of 0.07436 mm using the II x-ray detector operating at 210 kV and 0.11 µA. This produced a set of 300 slices at 1024 x 1024 resolution, covering approximately 22.308 mm of the basicranium, starting at the occipital condyles and ending just rostral to the petrosal.

Cranial morphologies were reconstructed from the CT scans using Amira 5.3 for Mac OS X (Visage, Inc., Chelmsford, MA: http://www.visage.com).

Comparative specimens (UCMZ 1989.47; UCZM 1975.496) were CT scanned at the Centre for Mobility and Joint Health, McCaig Institute for Bone and Joint Health, University of Calgary, using a Dual-energy CT/GSI (GE Revolution HD GSI, 140 kV and 80 kV fast switching).

Measurements—All measurements were taken using the 3D measurement tool of Amira. Basicranial length measurements were based on the protocols outlined by Janis [28]. Total skull lengths were measured from the tip of the rostrum to the caudal-most point of the occiput. Length and width measurements of the anterior semicircular canal were made following the protocol of Janis [28], and the arc radius was calculated using the equation provided by Ekdale [30]. Height and width measurements of the cochlea were made following Silcox et al. [31].

Body Mass Estimates—Body mass (BM) estimates were calculated for AMNH-VP 53523 but not AMNH-VP 1229. This is because most endocranial data comes from AMNH-VP 53523. Estimates for AMNH-VP 53523 were based on the predictive body mass regressions proposed by [28]. We used the “ruminants only” total skull length (SL) and basicranial length (BL)] regressions to estimate body mass. We chose to use the “ruminants only” regressions because the cranial

morphology of *P. celer* greatly resembles that of a ruminant [28]. The "all artiodactyls" regressions, particularly the total skull length regression, produced unrealistically large body mass estimates that conflict with prior results [28]. The two ruminant body mass equations used are:

$$Total\ skull\ length\text{:}\ \log_{10} BM\ (kg)\ = 2.969(\log_{10} SL) - 2.348$$

$$Basicranial\ length\text{:}\ \log_{10} BM\ (kg)\ = 3.218(\log_{10} SL) - 1.209$$

Agility Scores—Agility scores (AGIL) were calculated using the anterior semicircular canal radius (ASCR) "all mammals" predictive equation of Spoor et al. [29]. This is because only the anterior semicircular canal was preserved in enough to detail to measure the width and height. We used two body mass estimates, based on different cranial variables, in our calculations. This provided a range of likely agility scores. The anterior semicircular canal equation is:

$$ASCR\text{:}\ \log_{10} AGIL\ = 0.850 - 0.153(\log_{10} BM) + 0.706(\log_{10} ASCR)$$

Body mass in the AGIL predictive equation is in grams, whereas the body masses calculated from the Janis [28] regressions are in kilograms. As such, a simple conversion is required.

Results

The external morphology of *Protoceras* was thoroughly described by previous authors [2,8–10,18] so only a brief description of external morphology will be presented here. AMNH-VP 1229 is better preserved externally and AMNH-VP 53523 is better preserved internally. As such, descriptions are based on a composite of the two skulls, with external descriptions primarily based on AMNH-VP 1229 and endocranial descriptions primarily based on AMNH-VP 53523.

Rostrum, Orbit, and Cranial Vault

The preorbital region is long and narrow, comprising approximately 2/3 of the total skull length (Fig. 1). The nasal bones are small and the external nares are large, spanning the majority of the rostrum. The nasals meet at a pointed process above the external nares. AMNH-VP 53523 has rostral horn-like cranial appendages on the nasals (Fig. 1E-F).

There are facial vacuities on the rostrum at the level of P3 (Fig 1. C, F). These vacuities have a well-defined rostral margin and an indistinct caudal margin. On AMNH-VP 1229, the palatine canal opens as a small foramen on the ventrocaudal edge of the left facial vacuity. A crest extends from the ventrocaudal margin of the vacuity to the anterior margin of the orbit. The dorsal surface of this crest is textured. AMNH-VP 1229 has a distinct infraorbital foramen just rostral to the orbit (Fig. 1C).

The orbits are large with a complete postorbital bar. On AMNH-VP 53523, there are cranial appendages projecting upwards from the dorsal border of the orbits (Fig. 1E). The orbital bones are thin, and the sutures are difficult to distinguish. The lacrimal appears to be a large bone pierced ventrally by the lacrimal canal. The zygomatic arch slopes ventrally from the squamosal to the orbit (Fig. 1C). The interorbital area (comprising the frontals) is mostly flat with a slight caudal incline (Fig. 1C, F). Two distinct, bilateral crests originate from the interorbital region, one directed rostrally and the other directed caudally. The rostral crests extend anteriorly onto the nasals. The caudal crests originate at the dorsocaudal margin of the orbit and extend posteriorly as bilateral sagittal crests, eventually joining in the midline of the occiput and then intersecting with the shield-like nuchal crest. On AMNH-VP 53523, the sagittal crests become the parietal cranial appendages (Fig. 1E). The parietals are smooth with no

distinctive foramina or projections, except for a short zygomatic process that contributes to the postorbital bar.

The dentition of *P. celer* is fully described in previous publications [2,18]. Both skulls have canines; however, the canines of AMNH-VP 1229 are greatly reduced compared to those of AMNH-VP 53523 (Fig. 1 A, D). The palate is narrow and flat. The palatine crests and the pterygoid processes of the sphenoid are tall, and the internal nares are visible along the midline. The palatal region is mediolaterally constricted.

Squamosal

The glenoid fossa of the squamosal is mediolaterally elongate with a slightly convex articular surface (Fig. 1A, C and Fig. 2A). A small, non-pneumatized postglenoid process borders the glenoid fossa. The postglenoid foramen penetrates the caudal face of the postglenoid process. Internally, contact between the squamosal and the petrosal is interrupted by a sinus venosus temporalis (Fig 3C). The presence of a foramen jugular spurium, an opening for the sinus venosus temporalis, cannot be confirmed because the bony elements are not in tight articulation. The presence of a glenoid foramen cannot be confirmed for the same reason.

Fig 2. CT renderings of the basicranium of AMNH 53323.

(A) Ventral view. (B) Left lateral view. Abbreviations: Boc, basioccipital; Ect, ectotympanic; Exo; exoccipital; Pop; paroccipital process of exoccipital; Sq, squamosal.

Fig 3. Transverse CT slices of AMNH 53323 showing important morphological features.

(A) Slice 88. (B) Slice 107. (C) Slice 131. Abbreviations: Boc, basioccipital; Pet; petrosal

A large rostrocaudally directed canal runs through the ventral part of the squamosal, piercing the skull above the glenoid fossa. We identify this exit as the supraglenoid foramen

based on AMNH-VP 1229. A similar foramen could not be identified on the surface of AMNH-VP 53523, but the internal canal is clearly visible in CT cross-sections (Fig. 3A). The canal appears to terminate caudally around the rostral margin of the ectotympanic, but the exact point of termination is indistinct.

Ectotympanic

The lateral portion of the ectotympanic is present in AMNH-VP 53523. The ectotympanic comprises the entirety of the *Protoceras* auditory bulla [10], but the bullar portion of the bone is missing from the specimen. AMNH-VP 1229 has a superficially complete auditory bulla but the internal structures are not preserved (Fig 1A). The bulla is small and uninflated and the anteromedial side projects as a wide and blunt styliform process. The bullar portion of the ectotympanic sits between the squamosal, basioccipital, and paroccipital process of the exoccipital. There is a gap between the bulla and the basioccipital in AMNH-VP 1229, but no internal structures, including the petrosal, can be seen because of poor internal preservation.

The external auditory meatus is located between the postglenoid process and post-tympanic process of the squamosal (Fig. 2B). Both the squamosal and the ectotympanic contribute to the external auditory meatus; the rostral and ventral borders of the meatus are formed by the dorsal margin of the ectotympanic, and the dorsal and caudal borders of the meatus are formed by the squamosal (Fig 2B). There is a gap between the postglenoid process and the rostral face of the ectotympanic, but the caudal face of the ectotympanic and the post-tympanic process are in articulation. The ectotympanic extends as a compressed plate ventral

to the external auditory meatus. The ventral border of this plate is missing in both specimens, but CT scans of AMNH-VP 53523 show that the plate is filled with cancellous bone.

Bony Labyrinth

Sections of both the left and right bony labyrinths are preserved in AMNH-VP 53523. The left bony labyrinth is more complete and will be the basis of this description (Fig. 4). The cochlear canal makes approximately 2.75 turns (rotation of 990°), but the exact termination point of the apex cannot be identified. Several sections of the cochlear canal are infilled with sediment, obscuring the borders and making it unclear whether the basal and secondary turns naturally contact each other. The aspect ratio, calculated by dividing the height of the spiral by the width of the basilar turn [31], is approximately 0.80.

Fig 4. CT renderings of the bony labyrinth (and surrounding petrosal, upper images) of AMNH 53323.

(A) Medial (endocranial) view. (B) Rostral view. (C) Ventrolateral view.

The vestibule is represented by a slightly bulbous saccule (spherical recess) and utricle (elliptical recess). The saccule, which is a medial bulge extending from the fenestra vestibuli, is more inflated than the utricle. The utricle sits between the saccule and the anterior ampulla of the anterior semicircular canal. The anterior semicircular canal is the only semicircular canal fully preserved in the left bony labyrinth (Fig. 4). The posterolateral base of the lateral semicircular canal is present, but the path of the canal cannot be traced. No part of the posterior semicircular canal could be reliably identified; a structure identified as the medial portion of the vestibular aqueduct may include the root of the posterior semicircular canal, but this cannot be confirmed. Fragments of both the anterior and posterior semicircular canals,

including the common crus, are present in the right bony labyrinth. The right lateral semicircular canal could not be located.

The left anterior semicircular canal is sigmoidal and lies in more than one plane. The anterior portion of canal projects rostrally, throwing that part of the semicircular canal into a tight arc. The path of the canal is less curved posteriorly, becoming almost straight in the region of the common crus.

Other aspects of the bony labyrinth are discussed along with the morphology of the petrosal.

Petrosal

Most of the petrosal was captured in the high-resolution CT scan of AMNH-VP 53523 (Fig. 5). The caudal portion of the mastoid region (along with other caudal structures) was not included, but the morphology of the petrosal can still be described.

Fig 5. CT renderings of the left petrosal of AMNH 53323 in five orientations. (A) Lateral (tympanic) view. (B) Rostral view. (C) Medial (endocranial) view. (D) Ventrolateral view. (E) Ventral view. Abbreviations: Pr, promontorium; Tt, tegmen tympani.

The promontorium is hemi-ellipsoid with a well-rounded lateral face (Fig. 5A). A small epitympanic wing, which lacks a lateral process, projects rostrally from the anterior margin of the promontorium (Fig. 5A, C). The epitympanic wing is roughly triangular and forms the rostral-most part of the petrosal. A groove separates the epitympanic wing from the posteromedial flange, which begins just caudal to the epitympanic wing and projects ventrally from the lower margin of the promontorium (Fig. 5A). The rostral tympanic process is absent.

The promontorium lacks a transpromontorial sulcus and a stapedial artery sulcus. A circular, ventrocaudally directed fenestra cochleae opens at the caudal end of the promontorium (Fig. 5A, D). There is an indistinct caudal tympanic process posterior to the fenestra cochleae. The fenestra vestibuli is an oval opening dorsal to the fenestra cochleae, and a small secondary facial foramen lies just dorsal to the fenestra vestibuli (Fig. 4C and Fig. 5A, D). The path of the facial canal can be briefly traced internally from the secondary facial foramen**,** but quickly disappears. This may be because the facial canal, which transmits the facial nerve, drastically changes diameter or has been infilled with sediment.

A deep and circular fossa for the muscularis tensor tympani excavates the tegmen tympani just rostral to the fenestra vestibuli and the secondary facial foramen. The stapedial muscle fossa is a deep and wide depression directly caudal to the fenestra vestibuli and the secondary facial foramen (Fig. 5A). The stapedial muscle fossa terminates ventrally as the stylomastoid notch, which is the petrosal contribution to the stylomastoid foramen (Fig. 5A, D). In *P. celer*, the rest of the stylomastoid foramen is formed by the exoccipital and represents the exit of the facial nerve from the middle ear cavity.

On the pars canicularis, the tegmen tympani is moderately inflated with a distinctive, oval-shaped tegmen tympani fossa on the dorsomedial side (Fig. 5B). The tegmen tympani is pierced rostrally by a slit-like hiatus Fallopii (Fig. 4B and Fig. 5B). The path of the greater petrosal nerve can be traced from where it enters the foramen acusticum superius with the rest of the facial nerve to where it exits though the hiatus Fallopii (Fig. 4). The exact point at which the greater petrosal nerve diverges from the rest of the facial nerve cannot be located because the facial canal is incomplete. The greater petrosal nerve canal is slightly exposed at the rostral

end of the epitympanic recess, inside the fossa muscularis tensor tympani, just ventrolateral to where the nerve emerges through the hiatus Fallopii. This exposure may be the result of thin bone that has been eroded.

The lateral portion of the tegmen tympani curves ventrally to form the roof of the epitympanic recess, which is an elongated channel that originates caudal to the epitympanic wing and terminates at the stapedial muscle fossa (Fig. 5A, D). The epitympanic recess lacks a distinct fossa for the head of the malleus. A short crista parotica, situated caudal to the stapedial muscle fossa, separates the epitympanic recess from the mastoid region of the petrosal (Fig. 5A). The tympanohyal projects laterally from the crista parotica (Fig. 5A, D). The lateral border of the tympanohyal is indistinct and may either be broken or merged with the ectotympanic.

The mastoid region comprises more than half of the petrosal. The caudal part of the mastoid region was not captured in the high-resolution CT scan of AMNH-VP 53523, but the mastoid region is clearly large and wedge shaped (Fig. 5). As has been described previously [10], the mastoid region is exposed externally as a strip of bone sandwiched between the exoccipital and the squamosal (Fig. 2B). A mastoid plate is not present.

The tegmen tympani forms a right angle with the endocranial surface of the petrosal, and a short crista petrosa rostral to the subarcuate fossa separates the tegmen tympani fossa from the endocranial face (Fig. 5C). The internal acoustic meatus is deep with a smooth border. The foramen acusticum superius and foramen acusticum inferius are separated by a narrow crista transversa (Fig. 4A and Fig. 5C). The foramen acusticum inferius is large and opens caudally whereas the foramen acusticum superius is small and opens ventrally. A prefacial

commissure borders the dorsal side of the internal acoustic meatus, but no prefacial commissure fossa is present. The subarcuate fossa lies caudal to the internal acoustic meatus. The subarcuate fossa is wide and extremely shallow, appearing as a subtle depression in the petrosal. A petromastoid canal is present on the rostral border of the subarcuate fossa (Fig. 4 and Fig. 5C). Internally, the petromastoid canal passes just inside the arc of the anterior semicircular canal, terminating halfway between the endocranial face and tympanic face of the petrosal.

The vestibular aqueduct, which carried the endolymphatic duct, travels from the common crus of the semicircular canals to emerge on the endocranial surface of the petrosal, ventrocaudal to the subarcuate fossa (Fig. 4 and Fig. 5C). A basicapsular groove (=petrobasilar canal [7]) runs along the ventral border of the petrosal (Fig. 3B). The cochlear aqueduct, on the ventromedial surface of the petrosal, sits medial to the basicapsular groove and slightly caudal to the internal acoustic meatus (Fig. 4 and Fig. 5E). Internally, the cochlear aqueduct originates just medial to the fenestra cochleae and is directed posteriorly as a long, thin channel. The cochlear aqueduct housed the perilymphatic duct in life.

Exoccipital

The exoccipital of *P. celer* is dominated by a prominent paroccipital process that projects ventrolaterally, extending well beyond the ventral margin of the basioccipital (Fig. 2). A crest on the lateral side of the paroccipital process intersects with the nuchal crest. The mastoid portion of the petrosal is visible laterally as a narrow strip of bone between the ventral margin of the squamosal and the paraoccipital process. Based on AMNH-VP 1229, the paroccipital process and the ectotympanic bulla are in close contact (Fig. 1A).

Basisphenoid

The exact point of contact between the basioccipital and basisphenoid is ambiguous because of a transverse crack through the region on AMNH-VP 53523 (Fig. 1D). The basisphenoid is broad caudally and narrow rostrally, forming a rod that is bordered laterally by the pterygoid processes of the alisphenoid (Fig. 1A, D). The ventral surface of the basisphenoid has two longitudinal grooves, one on each side of the midline. The foramen ovale is externally visible on the left lateral side of AMNH-VP 1229, ventral to the otic region.

Basioccipital

The basioccipital is bounded dorsolaterally by the exoccipitals and rostrally by the basisphenoid. The basioccipital and exoccipitals are tightly sutured. The basioccipital is a robust bone with a groove running along the ventral midline (Fig. 2A). The large occipital condyles extend from the exoccipital onto the basioccipital with paired tubercles at their anteroventral margin (Fig. 2A). The dorsolateral border of the condyle is demarcated by a distinct grove, and the hypoglossal foramen is located on the dorsal aspect of this groove. The left side of both AMNH-VP 1229 and AMNH-VP 53523 has two adjacent foramina in this position, likely a separate hypoglossal foramen and condylar foramen.

A paired groove is present on the dorsolateral (endocranial) surface of the basioccipital where the basioccipital is close to contacting the ventral margin of the petrosal (Fig. 3B). This groove is interpreted as the basicapsular groove, which carries the inferior petrosal venous sinus. The groove is only present on the basioccipital for a small section, suggesting that the path of the sinus diverges from the bone rostrally.

Body Mass and Agility Scores

Body mass and agility scores were calculated for AMNH-VP 53523. The rostral to caudal skull length of AMNH-VP 535253 is 18.8 cm, and the basicranial length is 6.21 cm. These values provided body mass estimates of 27.3 kg and 22.0 kg, respectively, which fit into body mass ranges previously predicted for *P. celer* [28].

The width of the anterior semicircular canal is 5.48 mm and the height of the anterior semicircular canal is 5.15 mm—the arc radius is 2.66 mm. When applied to the appropriate agility predictive equation (see Materials and Methods), we recover two agility scores. Using the full skull length body mass, we predict an agility score of 2.97. Using the basicranial body mass, we predict an agility score of 3.057.

Discussion

Squamosal

Squamosal morphology is fairly conserved in protoceratids. Like others in the family, *P. celer* lacks a preglenoid process, has a slightly convex glenoid fossa, and has a low postglenoid process. A sinus venosus temporalis is present in both basal and derived protoceratids, and in several other artiodactyls including the oreodont *Merycoidodon culbertsoni* [32], the cainotheriid *Cainotherium* [33], and the camelids *Poebrotherium* and *Lama glama* [25,32]. The sinus venosus temporalis of the basal protoceratid *Leptotragulus* is reportedly larger than that of the derived protoceratid *Syndyoceras* and of non-protoceratids [7]. The sinus venosus temporalis of *P. celer* appears to be slightly larger than that of *Syndyoceras*, but distortion of the skull makes such comparisons difficult. It does not appear to be as large as the sinus venosus temporalis of *Leptotragulus*.

A supraglenoid foramen, similar to that of *Paratoceras*, is present in *P. celer* [2]. To our knowledge, these are the only protoceratid taxa for which a supraglenoid foramen has been reported. The lack of its identification in previous descriptions of *Protoceras* [10,18] suggests that the foramen may be variably present within the taxon. A supraglenoid foramen could not be identified on AMNH-VP 53523 even though sections of the internal canal leading to the foramen are present. This may be because of poor exterior preservation or may be a true absence. We have been unable to examine additional specimens and thus cannot comment on the general distribution of the supraglenoid foramen among protoceratids.

A foramen jugular spurium was reported in one specimen of *Leptotragulus* [7] but this foramen could not be located on the *P. celer* specimens.

External exposure of the petrosal (the mastoid condition) is common in selenodont artiodactyls, although the position and amount of exposure varies among taxa [32,34]. Typically, the mastoid sits between the squamosal dorsolaterally, the exoccipital ventrally, and the supraoccipital medially. The mastoid exposure of *P. celer* is normal in this regard, and is similar to that of other protoceratids in being a laterally-oriented thin band of exposed bone [7,25]. Both *P. celer* and *Syndyoceras* have the typical mastoid position [25]. Norris stated that the mastoid region of *Leptotragulus* lies between the squamosal and supraoccipital, but the paroccipital processes were missing from the specimens he examined [7]. It is unclear whether there would have been mastoid-exoccipital contact if the paroccipital processes were intact. Mastoid contact has not been described for other basal protoceratids, but based on an illustration of *Leptoreodon marshi*, the mastoid does contact the exoccipital [12]. Norris described the presence of a mastoid foramen on the dorsal border of the exposed mastoid

region [7]. The high-resolution CT scan of AMNH-VP 53523 does not extend far enough caudally to determine if a mastoid foramen is present, and we do not know of any published descriptions of *Protoceras* having a mastoid foramen.

Ectotympanic

The *P. celer* bulla is located between the squamosal, basioccipital, and paroccipital process of the exoccipital. This is typical of all protoceratids [2,25]. Joeckel and Stavas observed that *Syndyoceras* has a thin bony process extending from the basioccipital to the bulla [25]. No such process is found in *P. celer*, but this may be because of regional breakage. Scott reported that the bulla and basioccipital of *Protoceras* are too closely appressed for the petrosal to be visible through the gap [10]. There is a gap in AMNH-VP 1229, but the gap is filled with matrix and no internal structures can be observed. Scott noted that one *Protoceras* specimen had an enlarged gap because of basicranial distortion [10]. This may be the case for AMNH-VP 1229 as the specimen is dorsoventrally compressed.

The auditory bulla of *P. celer* is small and uninflated, a condition shared with all protoceratids [2,10,18,25]. Poor preservation of the bulla means that its internal structure cannot be determined, but previous authors have reported that *Protoceras* joins other protoceratids in having a hollow bulla [25]. Most ruminants (except tragulids) also have a hollow bulla, whereas camelids, cainotheriids, suiforms, and some merycoidodontids have a bulla filled with cancellous bone [25,32,33]. Like *Paratoceras* and *Syndyoceras*, the styliform process of *P. celer* is wide and blunt [2,25]. Other artiodactyls with small- or medium-sized bullae typically have a more slender styliform process [32].

The lateral ectotympanic contributes to the rostral portion of the external auditory meatus and the squamosal contributes to the dorsal and caudal portions. This construction is found in all protoceratids, as well as pecorans and the homacodontid *Bunomeryx* [2,7,25,35]. Conversely, the external auditory meatus of camelids is primarily formed by the ectotympanic, having only a slight dorsal contribution from the squamosal [32,36]. In cainotheriids, the squamosal does not contribute to the external auditory meatus at all [33].

The *P. celer* ectotympanic also extends as a ventral projection below the external auditory meatus. A similar ventral projection is present in *Syndyoceras* [25]. In both cases, the projection is filled with cancellous bone. Joeckel and Stavas posited that this projection might be homologous to the much larger "lateral plate" of the camelid bulla [25], but concluded that it could easily be an independent derivation as several artiodactyls have a similar structure [34]. The ventral projection of *P. celer* does not help to resolve this question of homology, but it does suggest that a cancellous ventral projection is common in protoceratids.

Bony Labyrinth

To our knowledge, this is the first published description of a protoceratid bony labyrinth. The bony labyrinth morphology of other purported tylopods is not well-known; morphologies have only been described from *Cainotherium* [33,37], *Diplobune* [38], and *Bathygenys* [39]. However, there have been extensive descriptions of extinct and extant ruminant bony labyrinths [40–44], and the bony labyrinths of the early artiodactyl *Diacodexis ilicis* and the extant suid *Sus scrofa* have also been described [39,45].

The cochlea of *P. celer* has 2.75 turns, which is more turns than *Diplobune*, moschids, cervids, and bovids, but fewer turns than *Cainotherium* and *S. scrofa* [37,38,40,44]. It is most

455 comparable to the tragulids; most tragulids have 3.0 turns or more, but *Moschiola meminna*
456 can range from 2.75 to 3.25 turns [41,42,45]. Cochlear coiling within a species often varies by
457 0.5 turns [42]. Using this range, the cochlea of *P. celer* is comparable to most artiodactyls,
458 excluding *D. ilicis*, *Bathygenys*, and *S. scrofa*.

459 The *P. celer* cochlea has an aspect ratio of 0.80. Anything above 0.55 is considered to be
460 a high aspect ratio, generally associated with "sharp-pointed" cochleae [31]. The aspect ratio of
461 *P. celer* is higher than that of other artiodactyls; the highest aspect ratio previously reported is
462 from a juvenile specimen of the tragulid *Hyemoschus aquaticus* (aspect ratio: 0.75), which also
463 has 2.75 cochlear turns [42]. Aspect ratios can vary within a species; other juvenile specimens
464 of *H. aquaticus* have aspect ratios as low as 0.62, and adult *H. aquaticus* specimens have aspect
465 ratios ranging from 0.57-0.62 [42]. A high aspect ratio is derived for artiodactyls, with basal
466 forms having ratios under 0.55 [39,45]. The high aspect ratio of *P. celer* is likely the result of a
467 tightly coiled basal turn rather than a high number of coils.

468 The vestibule of *P. celer* is typical of artiodactyls. Most taxa have a slightly inflated
469 saccule and utricle with a clear distinction between the two structures [e.g., 38,41,45], although
470 this is not the case of *Bathygenys* [39]. The vestibular aqueduct appears to originate from the
471 common crus, but the medial end of the aqueduct could not be identified in *P. celer*.
472 Artiodactyls generally have a vestibular aqueduct that originates either at the base of the
473 common crus or just anterior to the common crus [e.g., 38,41,45], so the position of the *P.*
474 *celer* vestibular aqueduct is as expected. Not much can be said about the morphology of the
475 semicircular canals given that only one canal is preserved in AMMH-VP 53523.

476 **Petrosal**

The *P. celer* petrosal is typical of protoceratids. It lacks the ventromedial flange characteristic of camelids, *Bunomeryx*, and *Cainotherium* (see 'Comparisons: Basioccipital' for further discussion), [7,25,33,35], and there is an endocranial ridge separating the cerebral and cerebellar faces (Fig. 3A), a feature shared with other protoceratids, with ruminants, and with anoplotheriids (Fig. 6) [7,25,38,46]. The presence of this ridge in *P. celer* indicates that a clear cerebral/cerebellar division was maintained throughout protoceratid evolution. This morphology has been used as evidence that protoceratids should be allied with ruminants [7,25], but the distribution of this morphology is not well-documented in other artiodactyl groups.

Fig 6. Transverse CT slices of *Protoceras*, a ruminant, and camelid showing differences in the endocranial ridge.

(A) Slice 88 of *Protoceras celer*, AMNH-VP 53523. (B) Slice 633 of *Muntiacus* (ruminant), UCMZ 1989.47. (C) Slice 338 of *Camelus dromedarius* (camelid), UCZM 1975.496.

Like other protoceratids, the subarcuate fossa of *P. celer* is a shallow depression on the endocranial face, and there is no mastoid fossa. The subarcuate fossa houses the paraflocculus of the cerebellum in life [47]. The depth of the subarcuate fossa varies among artiodactyls, and the shallow nature of the protoceratid subarcuate fossa has been used as an argument for uniting protoceratids with pecoran ruminants [7,25]. This is because pecoran ruminants also have a shallow subarcuate fossa, whereas the camelids *Poebrotherium* and *Lama glama* have a deep subarcuate fossa [25,26,44]. Within Artiodactyla, camelids are unusual in having a deep subarcuate fossa, but they are not the only exception: the early artiodactyls *Bunomeryx*, *Diacodexis ilicis*, *Dichobune*, and *Gobiohyus* also have a deep subarcuate fossa [35,48], as do the

basal ruminants *Leptomeryx, Archaeomeryx*, and members of the Hypertragulidae [20,26], the basal suoid *Perchoerus* and members of the Palaeochoeridae [26,49], and members of the endemic European Cainotheriidae and Anoplotheriidae [33,37,38]. The extant ruminant *Tragulus napu* and the extant suid *Babyrousa babyrussa* also have a deep subarcuate fossa [26]. Furthermore, the extant camelid *Camelus dromedarius* has a shallow subarcuate fossa [26]. This character state distribution suggests that, while a shallow subarcuate fossa is shared between protoceratids and pecoran ruminants, this morphology may have evolved independently several times.

Perhaps a more compelling argument for a close relationship between protoceratids and ruminants—or the lack of a close relationship between protoceratids and camelids—is the absence of a mastoid fossa in protoceratids. The mastoid fossa is an indentation in the subarcuate fossa that houses the lobulus petrosus of the cerebellum [32]. Within Artiodactyla, it is only known from camelids [32], the homacodontid *Bunomeryx* [35], and the endemic European artiodactyls *Cainotherium*, *Anoplotherium*, *Dichobune*, and *Xiphodon* [33,37,46,50]. Like the shallow subarcuate fossa, the lack of a mastoid fossa in protoceratids has been used to suggest that protoceratids are more closely allied with ruminants than with camelids [7,25].

There are a few differences between *P. celer* and other protoceratids. *Leptotragulus* has a rostral tympanic process, a thick rim of bone bordering the ventrolateral pars cochlearis below and behind the promontorium [7]. The size of this process may have caused the *Leptotragulus* fenestra cochleae to be ventrally oriented [7]. A similarly enlarged rostral tympanic process and ventrally-oriented fenestra cochleae are present on the basal ruminants *Hypertragulus*, *Archaeomeryx*, and *Leptomeryx* [20]. No such enlarged rostral tympanic process

is found on *P. celer* or the more derived protoceratid *Syndyoceras* [25]. However, the fenestra cochleae of *P. celer* opens ventrally like that of *Leptotragulus*. This suggests that an enlarged rostral tympanic process may be the ancestral condition for protoceratids, and that the ventral orientation of the fenestra cochleae was retained for some time after the rostral tympanic process was reduced.

Protoceras celer has a tegmen tympani fossa, which is a rostrally-directed depression on the tegmen tympani that opens towards the cerebral cavity [48]. The early artiodactyls *Diacodexis*, *Dichobune*, and *Homacodon* also have this condition [48]. Orliac and O'Leary suggested that the tegmen tympani fossa received part of the temporal lobe of the cerebrum and the trigeminal ganglion for the trigeminal nerve [51]. A tegmen tympani fossa has not been explicitly documented in other protoceratids, but Joeckel and Stavas described a well-developed shelf-like process at the rostromedial border of the *Syndyoceras* petrosal [25]. This process forms the dorsolateral border of an alisphenoid groove that may have transmitted the trigeminal nerve or ganglion [25]. *Protoceras celer* lacks such a process and does not have any structures that roof the alisphenoid in the manner depicted in CT scan of *Syndyoceras* [25]. Joeckel and Stavas suggested that *Syndyoceras* was displaying a basal artiodactyl condition because neither camelids nor ruminants are known to have a similar shelf-like rostral process [25]. Given that the process is not present in more basal protoceratids such as *P. celer*, it is more likely that that this shelf-like process is a derived condition. The morphology of *P. celer* may be the precursor to the more elaborate morphology of *Syndyoceras*—if the latter has a tegmen tympani fossa (which cannot currently be determined), the fossa may be expended rostrally and medially to border the alisphenoid canal. This would be in line with the

543 suppositions of previous researchers that both structures are in close association with the
544 trigeminal ganglion [25,51].

545 *Protoceras celer* differs from both *Leptotragulus* and *Syndyoceras* in possessing a
546 petromastoid canal [7,25]. This canal transmits the subarcuate artery [52], and the path of the
547 canal can be clearly followed in the high-resolution CT scan of AMNH-VP 53523. The presence
548 of a petromastoid canal has evolved several times in artiodactyls; it is present in extant
549 hippopotamids, some suoids, and *C. dromedarius* [26], as well as several dichobunoids [48],
550 several extinct suoids [49], the oreodont *Merycoidodon* [26], and the anoplotheriid *Diplobune*
551 [38]. A petromastoid canal is also found in the mesonychid *Dissacus* [53]. Orliac and O'Leary
552 suggested that the widespread presence of the petromastoid canal in early artiodactyls may
553 indicate that it is an artiodactyl plesiomorphy [51]. If so, then *P. celer* has either retained or
554 independently re-evolved a primitive condition that has been lost in other protoceratids.

555 **Exoccipital**

556 The exoccipital of *P. celer* is like that of other protoceratine protoceratids [2].
557 *Syndyoceras* has a tight articulation between the paroccipital processes and the auditory bulla
558 [25]. *Protoceras celer* also has a close contact between the structures, but we cannot comment
559 on whether there is fusion because the bullar portion of the ectotympanic is missing in AMNH-
560 VP 53523 and the CT scan of AMNH-VP 1229 is not of high enough resolution.

561 **Basisphenoid**

562 *Syndyoceras* has a ventral midline groove running along the basioccipital onto the
563 basisphenoid [25]. There is a midline groove present on the basioccipital of AMNH-VP 53523,
564 but we cannot determine whether it continues onto the basisphenoid because the point of

565 contact between the two bones in indistinct. A pair of ventral grooves bordering the
566 basisphenoid midline, just rostral to the termination of the original midline groove, was figured
567 for *Syndyoceras* [25]. These grooves are present on AMNH-VP 53523.

568 **Basioccipital**

569 The basioccipitals of *Protoceras* and *Syndyoceras* have been reported to be similar in
570 shape and structure [25]. We concur with this assessment, although we do note some
571 additional features. Both AMNH-VP 1229 and AMNH-VP 53523 have separate hypoglossal and
572 condylar foramina on the left side of the skull. Separate foramina are not uncommon, and this
573 separation often occurs on only one side of the skull. Such variation is present on specimens of
574 *Ovis* and *Lama* (pers. obvs.) and have also been documented on the mesonychid *Dissacus* [54].

575 *Syndyoceras* has a pronounced basicapsular groove on the dorsolateral surface of the
576 basioccipital (Fig. 7E) [25]. This groove likely carried the inferior petrosal venous sinus.
577 *Protoceras celer* also has a basicapsular groove, but it is less pronounced. There is a faint
578 complementary groove on the ventral surface of the petrosal, suggesting that the inferior
579 petrosal venous sinus was cradled between the two bones rather than located solely on the
580 basioccipital (Fig. 7D). *Protoceras celer* may be displaying an intermediate condition; Norris
581 described a similar groove on the ventromedial surface of the *Leptotragulus* petrosal, but there
582 was no discussion as to whether an accompanying basioccipital groove was present [7].
583 *Syndyoceras* has a small, paired sinus in the dorsal basioccipital, adjacent to the auditory bulla
584 and immediately posterior to the basicapsular grooves. No such sinuses are present in *P celer*.
585 Joeckel and Stavas suggested that this paired sinus was the caudal portion of the inferior

586 petrosal venous sinus [25]. If so, the absence of this sinus in *P. celer* further indicates the minor
587 association between the inferior petrosal venous sinus and the basioccipital.

588 **Fig 7. Diagrammatic basicranial cross-sections showing the basicapsular groove position in**
589 **various artiodactyl families.**

590 (A) *Lama pacos* (ZM 16018), a camelid. (B) An unidentified ruminant. (C) *Cainotherium*
591 *commune* (YPM 25037), a cainotheriid. (D) *Protoceras celer* (AMNH 53523), an intermediate
592 protoceratine protoceratid. The bullar portion of the ectotympanic is absent in this specimen.
593 (E) *Syndyoceras cooki* (USNM 1153), a derived synthetoceratine protoceratid. The CT slice
594 depicted here is relatively rostral compared to the other taxa; the basicapsular groove does not
595 appear to extend farther caudally [25]. The black circle represents the basicapsular groove.
596 Abbreviations: Ab, auditory bulla; Boc, basioccipital; Pet, petrosal. A, B, and E are after Norris
597 [35], C is after Theodor [33].

598 The difference in basicapsular groove location between *Syndyoceras* and *P. celer* potentially
599 has phylogenetic significance. Most extant artiodactyls have an inferior petrosal venous sinus
600 that passes through the space between the auditory bulla and basioccipital [35]. Conversely,
601 camelids, *Merycoidodon*, and *Bunomeryx* have an inferior petrosal venous sinus that is
602 sandwiched between the basioccipital and the petrosal, much like the sinus of *P. celer* [32,35]
603 (Fig. 7). The petrosal-basioccipital location of the sinus has been previously proposed as a
604 tylopod synapomorphy [35]. *Cainotherium* and *Syndyoceras* appear to be the extremes of this
605 condition; *Cainotherium* carried the inferior petrosal venous sinus entirely on the petrosal, and
606 *Syndyoceras* carried the inferior petrosal venous sinus entirely on the basioccipital (Fig. 7)
607 [25,33]. The confinement of the inferior petrosal venous sinus to the basioccipital has been

used as evidence against a tylopodan affiliation for *Syndyoceras* and protoceratids as a whole [25]. The discovery that *P. celer*, a protoceratid basal to *Syndyoceras*, has a petrosal-basioccipital location for the sinus brings this conclusion into question. However, such a position does not necessitate that protoceratids are tylopods. Camelids and *Bunomeryx* both have a prominent ventromedially directed "flange" on the petrosal that roofs the basicapsular groove [25,35]. *Leptotragulus* and *P. celer* lack such a flange; the ventral border of the petrosal is rounded in both taxa [7]. This suggests that the petrosal-basioccipital condition observed in *P. celer* may be independently derived. The small size and short length of the basicapsular groove on the basioccipital could indicate that the inferior petrosal venous sinus was in the process of migrating from an unknown ancestral condition to the derived condition of *Syndyoceras* (Fig. 7). Several extant ruminants, all lacking a ventromedial flange, have a basicapsular groove on the petrosal [26], so the presence of such a groove on *Leptotragulus* is not particularly informative. The endocranial morphology of more basal protoceratids will need to be examined to determine what the ancestral protoceratid condition may be.

Agility Scores of *P. celer*

The completeness of the AMNH-VP 53523 left anterior semicircular canal allowed us to estimate an agility score for *P. celer*. The estimated scores, based on two body mass predictions, were 2.97 and 3.057. Agility scores are integer values that can range from 1 to 6, with 1 corresponding to the least agile mammals (e.g., sloth) and 6 corresponding to the most agile mammals (e.g., squirrel) [30]. The cursorial artiodactyl *Gazella bennetti* has an agility score of 3.37 while the slower moving artiodactyl *S. scrofa* has an agility score of 2.53 [29]. An intermediate artiodactyl, *Camelus dromedarius*, has an agility score of 2.67 [29]. These values

are derived from a predictive equation that incorporates all three semicircular canals. When only the anterior semicircular canal is used to calculate agility scores, as was necessitated for *P. celer*, *G. bennetti* has a score of 3.29, *C. dromedarius* has a score of 2.73, and *S. scrofa* has a score of 1.85; the scores have a slightly larger range but are still comparable [29]. Based on these data, the agility scores of *P. celer* suggest that it was an intermediate to slightly cursorial animal, an interpretation that is supported by its postcranial morphology.

The Identity of AMNH-VP 645

In her monograph on artiodactyl petrosals, O'Leary described and figured a petrosal, AMNH-VP 645, referred to *P. celer* [26]. The skull of AMNH-VP 645 was previously assigned to *P. celer* [2], but we cannot determine whether the AMNH-VP 645 petrosal belongs to the same individual; to our knowledge, there is no record of the petrosal being collected in association with the skull or being dissected out of the skull after collection. The AMNH-VP 645 petrosal closely resembles that of the basal camelid *Poebrotherium* but is in direct contrast to the morphology described for basal (*Leptotragulus*) and highly derived (*Syndyoceras*) protoceratids, implying reversals in the interpretation of several characters such as the presence of a deep subarcuate fossa. Our description of an *in-situ* petrosal of *P. celer* (AMNH-VP 53523) is in line with the morphology of other protoceratids and contrasts with the morphology of AMNH-VP 645. Given that the identity of AMNH-VP 53523 is unquestionably *P. celer*, we suggest that the AMNH-VP 645 petrosal is either an incredibly aberrant specimen, or, more likely, was assigned to *P. celer* in error. A re-examination of the specimen could provide clarification.

Conclusion

Basicranial morphology, particularly petrosal morphology, has repeatedly been used as evidence for a close relationship between protoceratids and ruminants. These characters include the presence of an endocranial ridge, the lack of a ventromedial flange, the shallow subarcuate fossa, and the lack of a mastoid fossa. However, none of these features are unique to protoceratids and ruminants. The basicranial morphology of *P. celer*, an intermediate protoceratid, is similar to both basal (*Leptotragulus*) and derived (*Syndyoceras*) forms, suggesting that basicranial morphology is conserved in the family. *Protoceras celer* exhibits some intermediate conditions which align with the hypothesized phylogenetic position of the taxon [4]; the basicrania of *P. celer* may document a transition in the orientation of the fenestra cochleae and the position of the basicapsular groove. *Protoceras celer* also possesses a petromastoid canal, which is an as-yet undocumented structure in protoceratids. The petromastoid canal is highly homoplastic in artiodactyls so the presence of such a structure in *P. celer* is not wholly surprising. The basicranial morphology of *P. celer* does not greatly illuminate the evolutionary relationships between protoceratids and other selenodont artiodactyls; however, the morphology of *P. celer* indicates that protoceratid basicrania did not undergo drastic changes during their evolution, despite derived members of the family acquiring extreme morphologies in other regions of the skull.

Acknowledgments

We thank C. Norris and J. Galkin at the American Museum of Natural History, New York, and W. Fitch at the University of Calgary for access to specimens, and A. Mellone at the American Museum of Natural History, New York for consultation and images of AMNH-VP 645. We thank M. Colbert and A. Mote at the High-Resolution C-Ray CT Facility, University of Texas at Austin,

for scanning and initial image processing of AMNH-VP 1229 and AMNH-VP 53523, and G. McRae, I. Pauchard, Y. Zhu, J. Allan, and A. Cooke at the Centre for Mobility and Joint Health, University of Calgary, for scanning UCMZ 1989.47 and UCMZ 1975.496. We acknowledge that the specimens we used in this study were collected from the ancestral lands of the Lakota Sioux people.

References

1. Norris CA. The cranium of *Leptotragulus*, a hornless protoceratid (Artiodactyla: Protoceratidae) from the Middle Eocene of North America. J Vertebr Paleontol. 2000;20(2):341–8.
2. Webb SD. *Kyptoceras amatorum*, new genus and species from the Pliocene of Florida, the last protoceratid artiodactyl. J Vertebr Paleontol. 1981;1(3–4):357–65.
3. Patton TH, Taylor BE. The Protoceratinae (Mammalia, Tylopoda, Protoceratidae) and the systematics of the Protoceratidae. Bull Am Museum Nat Hist. 1973;150:351–413.
4. Janis C. Evolution of horns in ungulates: ecology and paleoecology. Biol Rev. 1982;57(2):261–318.
5. Prothero DR. Protoceratidae. In: Janis CM, Scott KM, Jacobs LL, editors. Evolution of Tertiary Mammals of North America, Volume 1, Terrestrial Carnivores, Ungulates, and Ungulate-like Mammals. Cambridge: Cambridge University Press; 1998. p. 431–8.
6. Prothero DR, Ludtke JA. Family Protoceratidae. In: Prothero DR, Foss SE, editors. The Evolution of Artiodactyls. Baltimore: The Johns Hopkins University Press; 2007. p. 169–76.
7. Patton TH, Taylor BE. The Synthetoceratinae (Mammalia, Tylopoda, Protoceratidae). Bull

Am Museum Nat Hist. 1971;145:123–218.

8. Marsh OC. A horned artiodactyle (*Protoceras celer*) from the Miocene. Am J Sci. 1891;41(241):5a-6a.

9. Osborn HF, Wortman JL. Characters of *Protoceras* (Marsh), the new artiodactyl from the Lower Miocene. Bull Am Museum Nat Hist. 1892;18:351–71.

10. Scott WB. The osteology and relationships of *Protoceras*. J Morphol. 1895;2(2):303–63.

11. Scott WB. The selenodont artiodactyls of the Uinta Eocene. Trans Wagner Free Inst Sci. 1899;6:1–120.

12. Wortman JL. The extinct Camelidae of North America and some associated forms. Bull AMNH. 1898;10:1–141.

13. Matthew WD. Notice of two new genera of mammals from the Oligocene of South Dakota. Bull Am Museum Nat Hist. 1905;21:21–6.

14. Colbert EH. The osteology and relationships of *Archaeomeryx*, an ancestral ruminant. Am Museum Novit. 1941;1135:1–24.

15. Stirton RA. Comments on the relationships of the cervoid family Palaeomerycidae. Am J Sci. 1944;242(12):633–55.

16. Simpson GG. The principles of classification and a classification of mammals. Bull Am Museum Nat Hist. 1945;85:1–350.

17. Janis CM, Theodor JM. Cranial and postcranial morphological data in ruminant phylogenetics. Zitteliana R B Abhandlungen der Bayer Staatssammlung für Paläontologie und Geol. 2014;32(32):15–32.

18. Scott WB. The Mammalian fauna of the White River Oligocene: Part IV. Artiodactyla.

Trans Am Philos Soc. 1940;28(4):363–746.

19. Stirton R. Relationships of the protoceratid artiodactyls and description of a new genus. Berkeley: University of California Press; 1967. 44 p.

20. Webb SD, Taylor EB. The phylogeny of hornless ruminants and a description of the cranium of Archaeomeryx. Bull Am Museum Nat Hist [Internet]. 1980;167(3):117–58. Available from: http://digitallibrary.amnh.org/dspace/handle/2246/1042%5Cnhttp://digitallibrary.amnh.org/dspace/bitstream/2246/1042/1//v2/dspace/ingest/pdfSource/bul/B167a03.pdf%5Cnhttp://digitallibrary.amnh.org/dspace/handle/2246/1042?show=full

21. Gentry AW, Hooker JJ. The phylogeny of the Artiodactyla. In: Benton MJ, editor. The Phylogeny and Classification of the Tetrapods, Volume 2: Mammals. Oxford: Clarendon Press; 1988. p. 235–72.

22. Gazin CL. A review of the upper Eocene Artiodactyla of North America. Smithson Misc Collect. 1955;128(8):1–96.

23. Wilson JA. Early Tertiary vertebrate faunas, Vieja Group and Buck Hill Group, Trans-Pecos Texas: Protoceratidae, Camelidae, Hypertragulidae. Texas Meml Museum, Univ Texas Austin. 1974;23:1–34.

24. Golz DJ. Eocene Artiodactyla of southern California. Nat Hist Museum Los Angeles Cty Sci Bull. 1976;26:1–85.

25. Joeckel RM, Stavas JM. Basicranial anatomy of *Syndyoceras cooki* (Artiodactyla, Protoceratidae) and the need for a reappraisal of tylopod relationships. J Vertebr Paleontol. 1996;16(2):320–7.

739 26. O'Leary MA. An anatomical and phylogenetic study of the osteology of the petrosal of
740 extant and extinct artiodactylans (Mammalia) and relatives. Bull Am Museum Nat Hist
741 [Internet]. 2010;335:1–206. Available from:
742 http://www.bioone.org/doi/abs/10.1206/335.1
743 27. Spaulding M, O'Leary MA, Gatesy J. Relationships of Cetacea (Artiodactyla) among
744 mammals: increased taxon sampling alters interpretations of key fossils and character
745 evolution. PLoS One. 2009;4(9):1–14.
746 28. Janis CM. Correlation of cranial and dental variables with body size in ungulates and
747 macropodoids. In: Damuth J, MacFadden BJ, editors. Body Size in Mammalian
748 Paleobiology: Estimation and Biological Implications. Canada: Cambridge University
749 Press; 1990. p. 255–300.
750 29. Spoor F, Garland T, Krovitz G, Ryan TM, Silcox MT, Walker A. The primate semicircular
751 canal system and locomotion. PNAS. 2007;104(26):10808–12.
752 30. Ekdale EG. Comparative anatomy of the bony labyrinth (inner ear) of placental mammals.
753 PLoS One. 2013;8(6):27–8.
754 31. Silcox MT, Bloch JI, Boyer DM, Godinot M, Ryan TM, Spoor F, et al. Semicircular canal
755 system in early primates. J Hum Evol [Internet]. 2009;56(3):315–27. Available from:
756 http://dx.doi.org/10.1016/j.jhevol.2008.10.007
757 32. Whitmore FC. Cranial morphology of some Oligocene Artiodactyla. United States Geol
758 Surv Prof Pap. 1953;243-H:117–60.
759 33. Theodor JM. Micro–computed tomographic scanning of the ear region of *Cainotherium*:
760 character analysis and implications. J Vertebr Paleontol. 2010;30(1):236–2.

761 34. Pearson HS. On the skulls of early Tertiary Suidae, together with an account of the otic
762 region in some other primitive Artiodactyla. Philos Trans R Soc London Ser B, Contain Pap
763 a Biol Character. 1927;215:389–460.
764 35. Norris CA. The cranium of *Bunomeryx* (Artiodactyla: Homacodontidae) from the Upper
765 Eocene Uinta deposits of Utah and its implications for tylopod systematics. J Vertebr
766 Paleontol. 1999;19(4):742–51.
767 36. Webb SD. The osteology of *Camelops*. Bull Los Angeles Cty Museum. 1965;1:1–54.
768 37. Hürzeler J. Osteologie und Odontologie der Caenotheriden. Abhandlungen der
769 Schweizerschen Palaeontol Gesellschaft. 1936;58–59:1–111.
770 38. Orliac MJ, Araújo R, Lihoreau F. The petrosal and bony labyrinth of *Diplobune minor*, an
771 enigmatic Artiodactyla from the Oligocene of Western Europe. J Morphol.
772 2017;278(9):1168–84.
773 39. Ekdale EG. Variation within the bony labyrinth of mammals. The University of Texas,
774 Austin, TX; 2009.
775 40. Mennecart B, DeMiguel D, Bibi F, Rössner GE, Métais G, Neenan JM, et al. Bony labyrinth
776 morphology clarifies the origin and evolution of deer. Sci Rep. 2017;7(1):1–11.
777 41. Mennecart B, Costeur L. A *Dorcatherium* (Mammalia, Ruminantia, Middle Miocene)
778 petrosal bone and the tragulid ear region. J Vertebr Paleontol. 2016;36(6):e1211665.
779 42. Mennecart B, Costeur L. Shape variation and ontogeny of the ruminant bony labyrinth,
780 an example in Tragulidae. J Anat. 2016;229(3):422–35.
781 43. Mennecart B, Rössner GE, Métais G, DeMiguel D, Schulz G, Müller B, et al. The petrosal
782 bone and bony labyrinth of early to middle Miocene European deer (Mammalia,

783 Cervidae) reveal their phylogeny. J Morphol. 2016;277(10):1329–38.

784 44. Costeur L. The petrosal bone and inner ear of *Micromeryx flourensianus* (Artiodactyla,

785 Moschidae) and inferred potential for ruminant phylogenetics. Zitteliana R B

786 Abhandlungen der Bayer Staatssammlung fur Palaontologie und Geol. 2014;32(32):99–

787 114.

788 45. Orliac MJ, Benoit J, O'Leary MA. The inner ear of *Diacodexis*, the oldest artiodactyl

789 mammal. J Anat. 2012;221(5):417–26.

790 46. Dechaseaux C. Artiodactyles primitifs des Phosphorites du Quercy II. Etude sur le genere

791 *Xiphodon*. Ann Paléontologie. 1967;53:27–47.

792 47. Gannon PJ, Eden AR, Laitman JT. The subarcuate fossa and cerebellum of extant

793 primates: comparative study of a skull-brain interface. Am J Phys Anthropol.

794 1988;77(2):143–64.

795 48. Orliac MJ, O'Leary MA. Comparative anatomy of the petrosal bone of dichobunoids, early

796 members of Artiodactylamorpha (Mammalia). J Mamm Evol. 2014;21(3):299–320.

797 49. Orliac MJ. The petrosal bone of extinct Suoidea (Mammalia, Artiodactyla). J Syst

798 Palaeontol. 2013;11(8):925–45.

799 50. Dechaseaux C. Artiodactyles primitifs des phosphorites du Quercy. Ann Paléontologie,

800 Vertebr. 1974;60:59–100.

801 51. Orliac MJ, O'Leary MA. Comparative anatomy of the petrosal bone of dichobunoids, early

802 members of Artiodactylamorpha (Mammalia). J Mamm Evol. 2014;21(3):299–320.

803 52. Mazzoni A. The subarcuate artery in man. Laryngoscope. 1970;80:69–79.

804 53. Luo Z, Gingerich PD. Terrestrial Mesonychia to aquatic Cetacea: transformation of the

805 basicranium and evolution of hearling in whales. Univ Michigan Pap Paleontol.
806 1999;31:1–98.
807 54. Geisler JH, Mckenna MC. A new species of mesonychian mammal from the lower Eocene
808 of Mongolia and its phylogenetic relationships Phylogenetic methods. Acta Palaeontol
809 Pol. 2007;52(1):189–212.
810

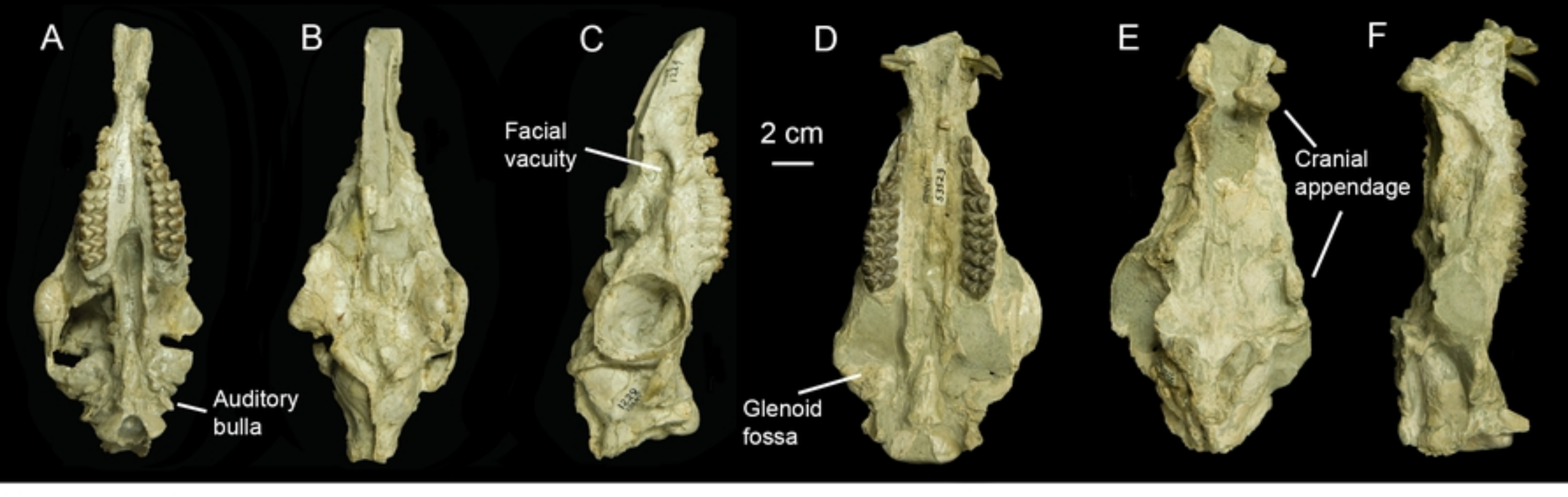
A
B
C
D
E
F
Auditory bulla
Facial vacuity
2 cm
Glenoid fossa
Cranial appendage

Figure1

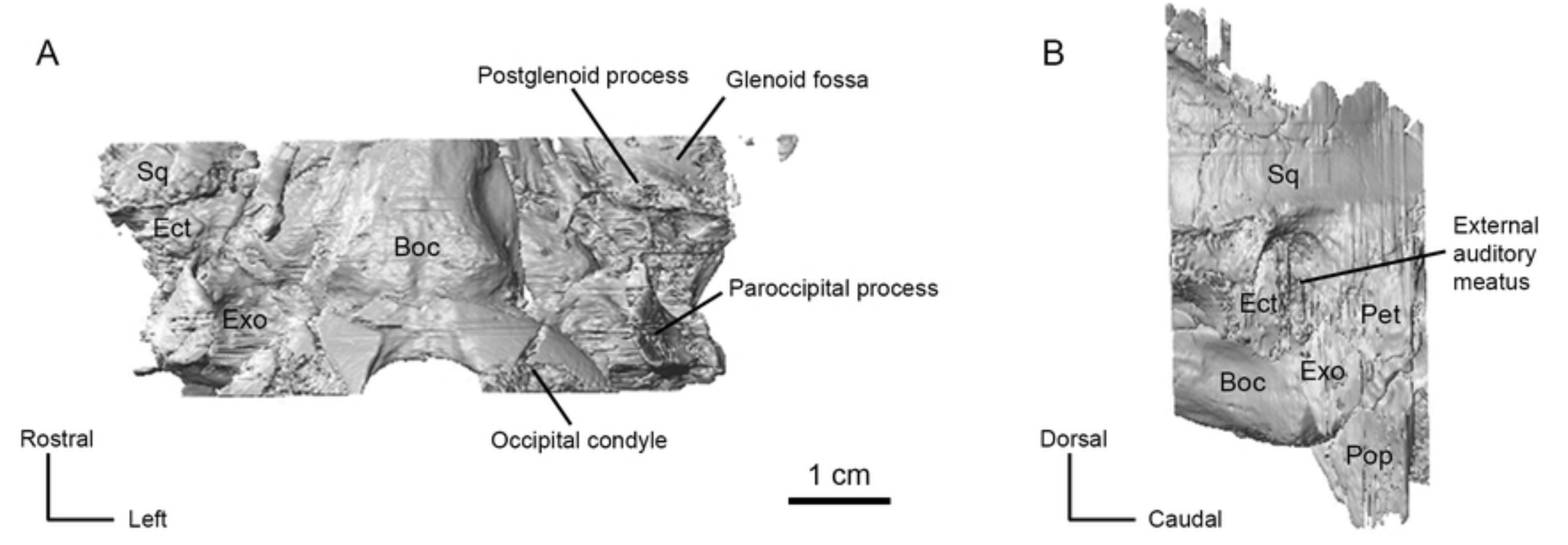
A
Postglenoid process
Glenoid fossa
Sq
Ect
Boc
Exo
Paroccipital process
Occipital condyle
Rostral
Left
1 cm
B
Sq
External auditory meatus
Ect
Pet
Boc
Exo
Pop
Dorsal
Caudal

Figure2

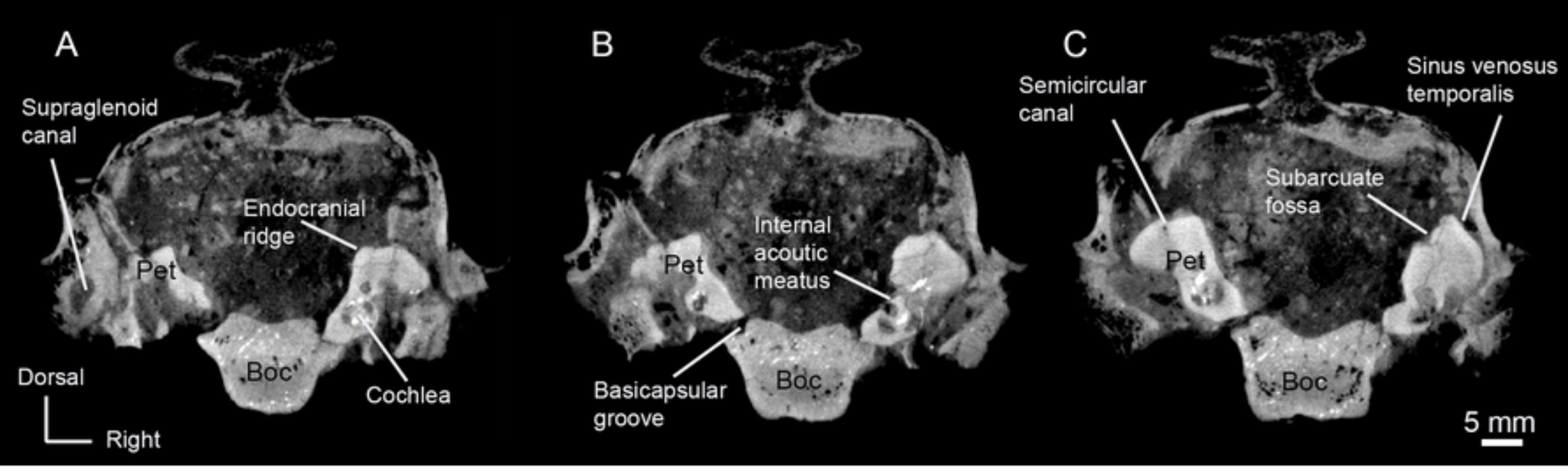
A
Supraglenoid canal
Endocranial ridge
Pet
Boc
Cochlea
Dorsal
Right
B
Pet
Internal acoutic meatus
Basicapsular groove
Boc
C
Semicircular canal
Sinus venosus temporalis
Subarcuate fossa
Pet
Boc
5 mm

Figure3

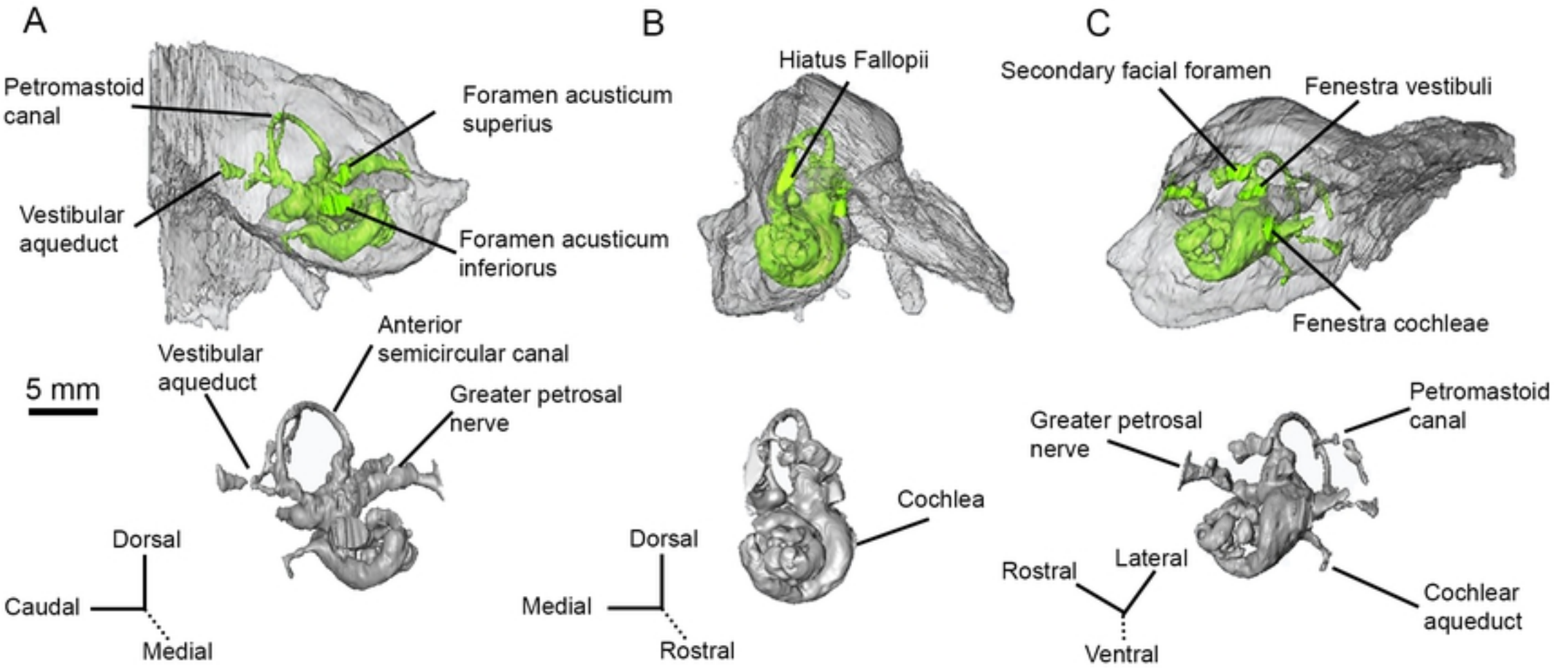
A
Petromastoid canal
Foramen acusticum superius
Vestibular aqueduct
Foramen acusticum inferiorus
Anterior semicircular canal
Vestibular aqueduct
Greater petrosal nerve
5 mm
Dorsal
Caudal
Medial
B
Hiatus Fallopii
Cochlea
Dorsal
Medial
Rostral
C
Secondary facial foramen
Fenestra vestibuli
Fenestra cochleae
Greater petrosal nerve
Petromastoid canal
Rostral
Lateral
Ventral
Cochlear aqueduct

Figure4

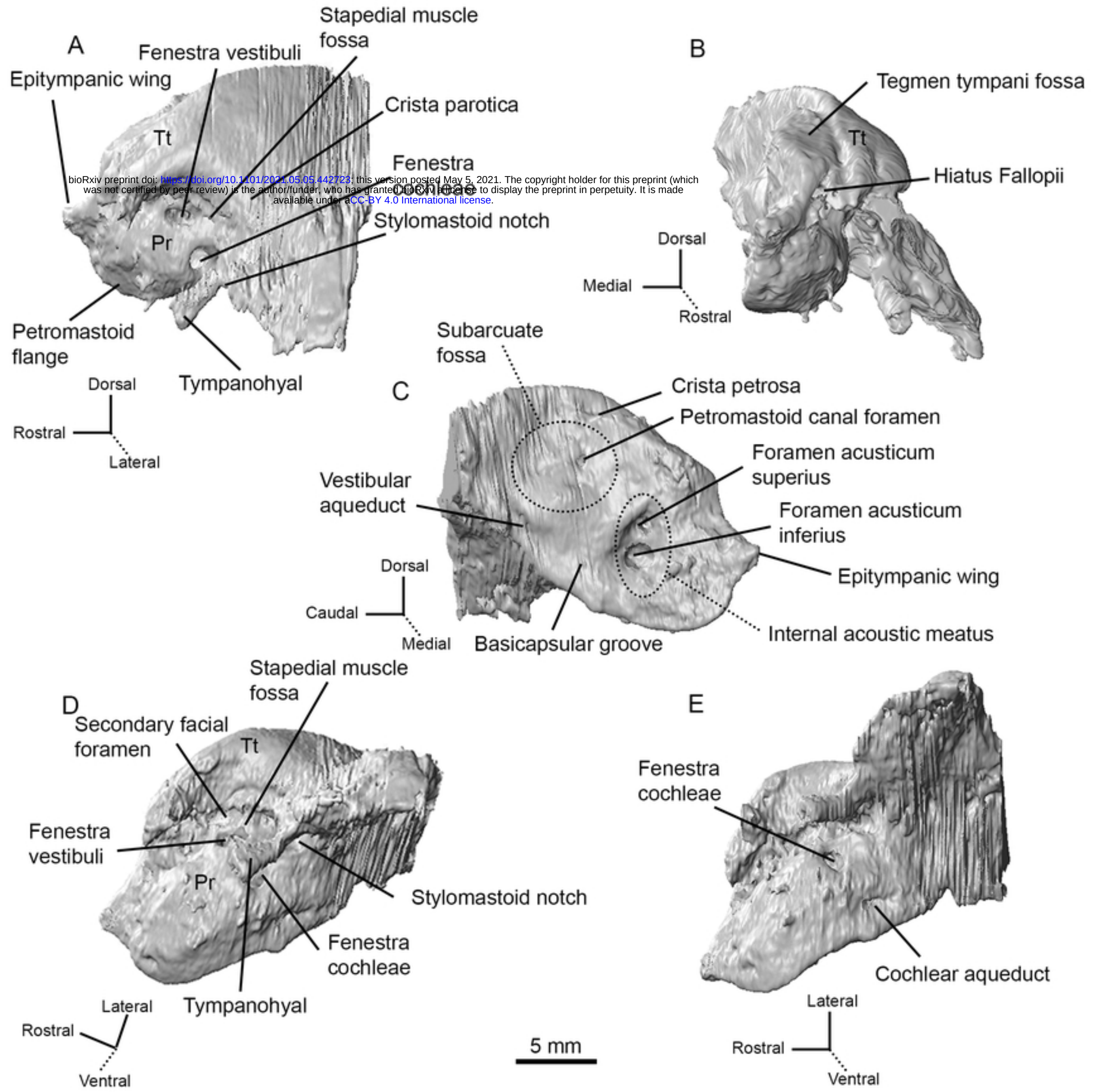

Figure5

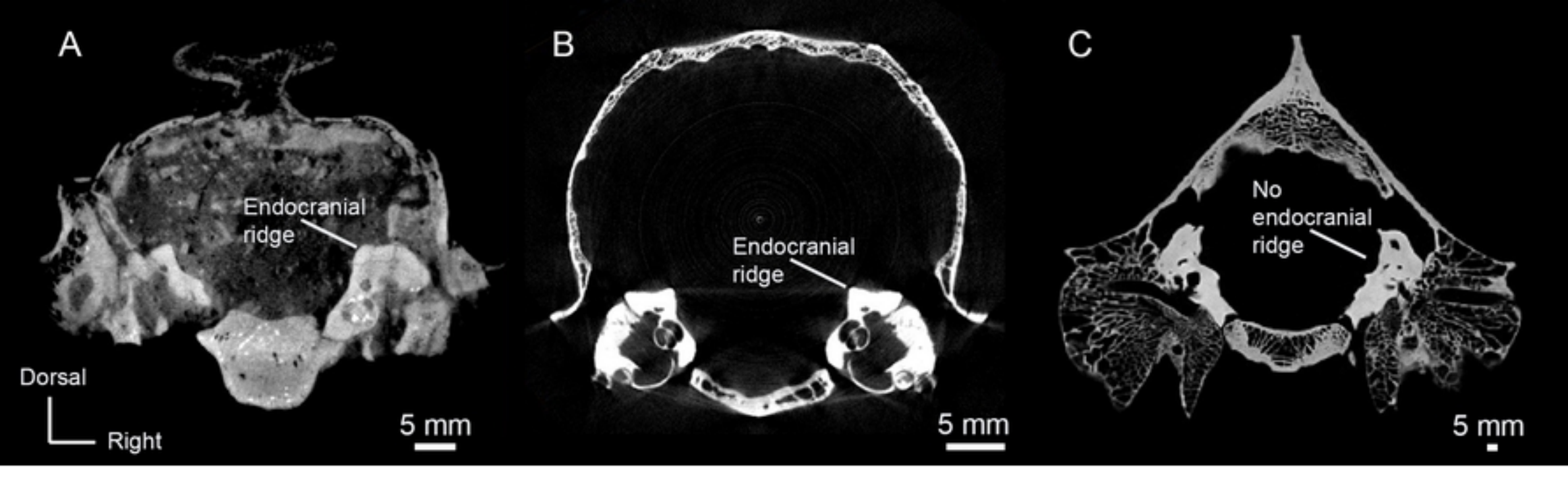
A
Endocranial
ridge
Dorsal
Right
5 mm
B
Endocranial
ridge
5 mm
C
No
endocranial
ridge
5 mm

Figure6

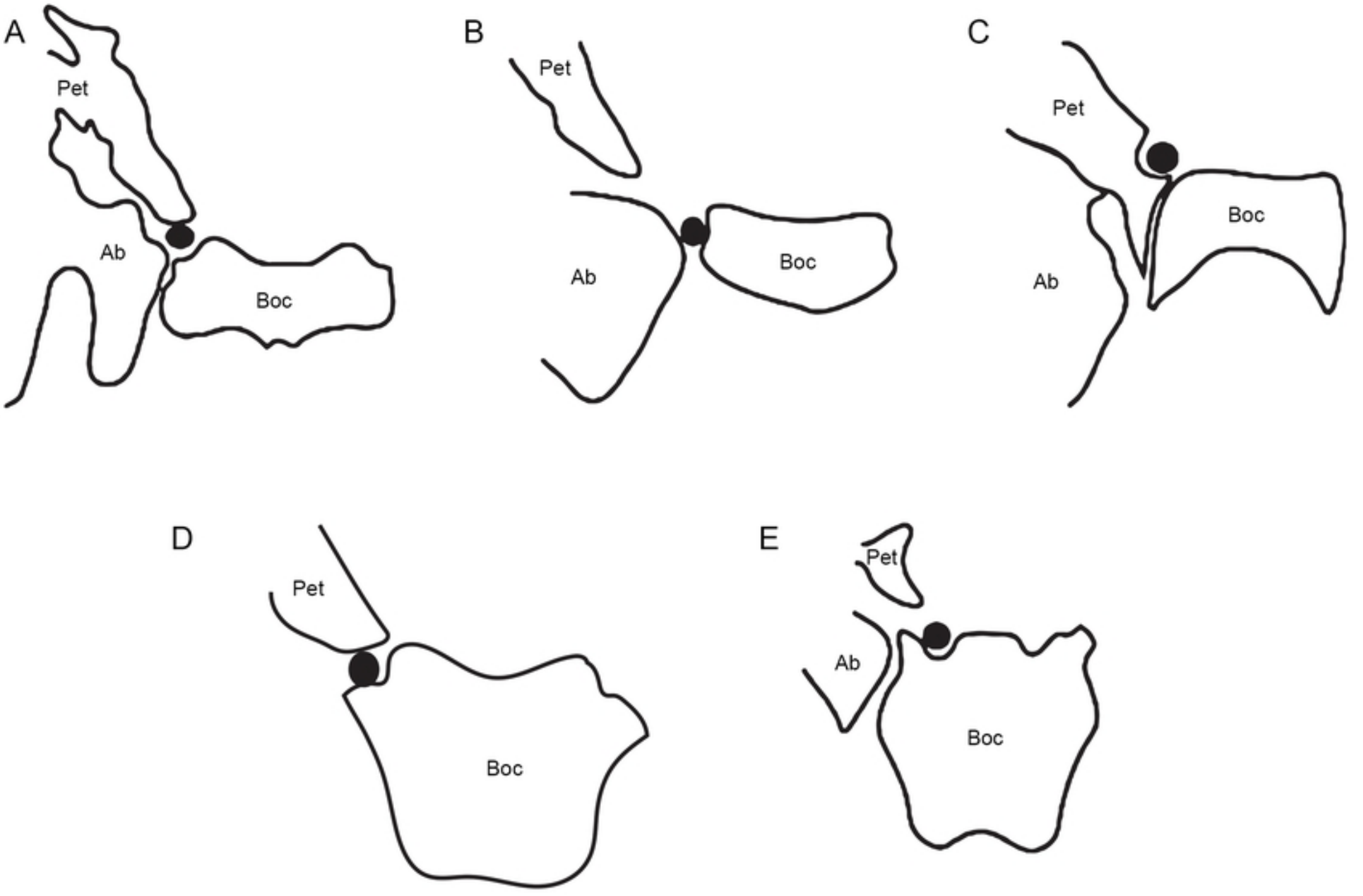

Figure7